An Experimental Study of Constant-Pressure Steam Injection and Transient Condensing Flow in an Air-Saturated Porous Medium

H. J. H. Brouwers
University of Twente,
Department of Civil Engineering & Management, P.O. Box 217,
7500 AE Enschede, The Netherlands

In this paper the unsteady process of constant pressure steam injection into an air-saturated porous medium is studied experimentally. To this end, vertical glass tubes are packed with dry quartz sand and injected with dry steam. The propagation of the steam front appears to be proportional to $\sqrt{t}$. It is observed that the water saturation is homogeneously distributed and remains below the irreducible water saturation. Furthermore, the theoretical model of Brouwers and Li (1994) of the process is applied to the experiments and extended to take wall effects into account. A comparison of the predicted front penetration and amount of condensed water with the experimental results yields fairly good agreement.

Introduction

Steam flow in porous media with heat transfer and condensation is encountered in many practical applications. Examples are steam injection enhanced oil recovery, geothermal energy production, drying processes, and cleaning contaminated soils.

Marx and Langenheim (1959) and Ramey (1959) were the first to model hot fluid injection into an oil reservoir. Mandl and Volek (1969) assessed the magnitude and importance of heat transfer ahead of the front and performed experiments. Based on the assumption of constant steam front velocity, Menegus and Udell (1985) and Stewart et al. (1989) also obtained an analytic expression, which agreed with their experiments. Morrison (1973) studied transient two-phase flow in porous media. Heat transfer ahead of the front was neglected and the governing equations were solved numerically. Based on a simple single-phase flow model, Brouwers and Li (1994) derived analytical expressions for transient condensing steam flow in a porous medium. Hanamura and Kaviany (1995) derived a constant-pressure steam injection model assuming a quasi-steady behavior and the presence of a liquid slug, and neglecting axial conduction in the dry air-saturated downstream region.

Constant-pressure injection experiments have been reported by Nilson and Montoya (1980), Tsuruta et al. (1988), and Hanamura and Kaviany (1995). Nilson and Montoya (1980) studied the injection of freon vapor into an initially dry sand pack. Tsuruta et al. (1988) and Hanamura and Kaviany (1995) investigated the injection of steam into a dry porous medium formed by packed glass beads. In both studies it was observed that if the condensate saturation is higher than the residual saturation, the superfluous condensate swept as a slug ahead of the steam front.

Constant-pressure steam injection and transient condensing flow in dry sand has, to the author's knowledge, never been reported. This situation is considered to be typical for the cleaning of the vadose zone of polluted subsoils. Accordingly, such experiments have been performed and the results are presented in this paper.

Contributed by the Heat Transfer Division for publication in the JOURNAL OF HEAT TRANSFER. Manuscript received by the Heat Transfer Division June 1995; revision received December 1995. Keywords: Condensation, Moving Boundaries, Porous Media. Associate Technical Editor: R. Viskanta.

Theory

In this section the analysis of Brouwers and Li (1994), concerning the one-dimensional longitudinal and unsteady propagation of the steam front, is recapitulated. The homogeneous and isotropic porous medium was considered to have a constant thickness and to be confined by impermeable and adiabatic top and bottom layers. The process studied involved the displacement of air by dry steam, which partly condenses to heat up the porous medium and initial groundwater.

Throughout their paper, it is assumed that the water saturation S_l is smaller than irreducible (residual or connate) water saturation S_{lr}, so that this liquid water is immobile. This water saturation consists of two parts, that is, the initial water saturation S_{l0}, which is zero, and the formed condensation water saturation S_{lc}. Thus it is assumed that

$$S_l = S_{lc} + S_{l0} < S_{lr} \tag{1}$$

It is noted that the assumption (1) is applicable because S_{lr} can amount to 20-25 percent (Buchlin and Stubos, 1991). Assumption (1) will be verified at the end of this section and in the experimental part of this paper.

The steam is injected at $x = 0$ at constant pressure. The steam flows through the unsaturated matrix to the condensation front (Fig. 1), the position of the front designated by $X_0(t)$, where the ambient pressure P_0 is attained.

There the condensation exists until the porous medium and the groundwater are heated up to the saturation temperature of the steam. It is assumed that the vapor, condensate, and matrix behind and in the front are in thermodynamic equilibrium, since the intraparticle thermal resistance and resistance from fluids to particles are both small.

The pressure drop between injection point and condensation front (typically 0.1 bar) is much smaller than the absolute pressure in the porous medium (ambient pressure), so that T_{sat} may be regarded as a constant. Hence, behind the steam front ($0 \leq x \leq X_0$), the temperature of the porous medium, water and steam, equals T_{sat}. Furthermore, a one-dimensional representation of the process was imposed by assuming the process to be uniform perpendicular to the direction of flow.

Based on an overall mass balance of water (steam and condensate), Darcy's law, and an energy balance at the steam front, the front position was obtained as

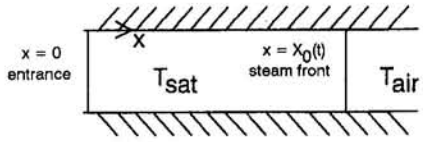

Fig. 1 Steam front position

$$X_0 = \sqrt{a_2}\lambda\sqrt{t} \tag{2}$$

where λ follows from

$$\sqrt{\pi}y \operatorname{erfc}(\lambda y)e^{\lambda^2 y^2} = \lambda \tag{3}$$

with

$$y = \left[\frac{a_2}{4a_1}\right]^{1/2} \equiv \left[\frac{\kappa H_{lat}(P_{in} - P_0)\kappa_{rv}}{2\overline{k}_s(T_{sat} - T_0)\nu_v}\right]^{1/2} \tag{4}$$

and

$$a_1 = \frac{\overline{k}_s}{\overline{\rho_s c_{ps}}} \tag{5}$$

and

$$a_2 = \frac{2\kappa_{rv}H_{lat}(P_{in} - P_0)\kappa}{\overline{\rho_s c_{ps}}(T_{sat} - T_0)\nu_v} \tag{6}$$

and erfc (x), the complementary error function, defined as:

$$\operatorname{erfc}(x) = 1 - \operatorname{erf}(x) = 1 - \frac{2}{\sqrt{\pi}}\int_{\eta=0}^{x} \exp(-\eta^2)d\eta \tag{7}$$

For a given y, which is determined by a_1 and a_2, λ can be determined as the root $\lambda(y)$ of Eq. (3). Subsequently, the steam-front position then follows from Eq. (2). Thus it is sufficient to know how $\lambda(y)$ changes versus y. The dimensionless group y is a measure for the latent heat transport by vapor flow divided by the heat conducted away ahead of the front.

Brouwers and Li (1994) computed $\lambda(y)$ numerically, the results of which are depicted in Fig. 2. Equation (4) reveals that the effect of condensed water in the porous medium on permeability was described with the concept of relative permeability.

The amount of condensed water in the porous medium was determined as:

$$S_{lc} = \frac{\overline{\rho_s c_{ps}}(T_{sat} - T_0)}{H_{lat}\phi\lambda^2\rho_l} \tag{8}$$

Equation (8) reveals that the amount of condensed steam does not depend on the position of the front. Hence, both the water saturation behind the front and the relative permeability of the steam are constant.

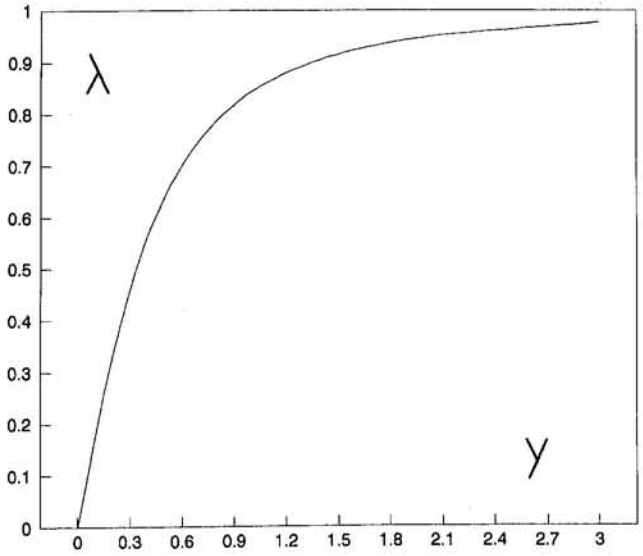

Fig. 2 Graphic representation of $\lambda(y)$

Experimental Results

One-dimensional steam injection experiments into an air-saturated dry sand pack were conducted for model comparison. Dry sand was chosen to avoid having the water saturation exceeding S_{ir}. Two pyrex glass tubes were used, one with a thin wall (tube I) and one with a thick wall (tube II); see Table 1. The length of the tubes (thickness of the packed bed) was about 1 m.

With each tube, two experiments were performed. The tubes were filled with dry quartz sand, because of the spherical grain size and nearly pure silica composition (≈99 percent). The particle size distribution of the sand is given in Table 2. From this distribution and the formula of Fair and Hatch (1933):

Table 1 Glass tubes used

Exp	Tube	D_i	D_o
1	I	50.0 mm	52.5 mm
2	I	50.0 mm	52.5 mm
3	II	51.0 mm	56.0 mm
4	II	51.0 mm	56.0 mm

Nomenclature

a_1 = thermal diffusivity, m^2s^{-1}
a_2 = parameter, Eq. (6), m^2s^{-1}
c_p = specific heat, $Jkg^{-1}K^{-1}$
D_i = inner diameter of the tube, m
D_o = outer diameter of the tube, m
d_p = mean particle size, m
H_{lat} = latent heat of condensation, Jkg^{-1}
k = thermal conductivity, $Wm^{-1}K^{-1}$
L = thickness of packed bed, m
n = power-law coefficient
P = pressure, Pa
S = saturation
T = temperature, K
t = time, s
u = superficial velocity, ms^{-1}
X_0 = position of steam front, m
x = coordinate, m
y = dimensionless group, Eq. (4)
β = parameter, Eq. (14)
η = dynamic viscosity, Pas
κ = absolute permeability, m^2
κ_r = relative permeability
λ = dimensionless parameter
ν = kinematic viscosity, m^2s^{-1}
ρ = density, kgm^{-3}
ϕ = porosity
ϕ = ωολθμε οφ ρατε< $\mu^{\times}\sigma^{-+}$

Subscripts

a = air
c = condensate
g = glass tube
in = injection
l = water
s = pertaining to sand and air
sat = saturation
v = vapor
0 = initial condition

Superscripts

$\bar{}$ = mean

Table 2 Particle size distribution

Diameter, μm	Mass fraction, percent
>300	2.92
250–300	36.08
212–250	30.21
150–212	28.33
125–150	1.78
90–125	0.39
63–90	0.05
<63	0.00

$$d_p = 0.78\left(\sum \frac{w_i}{d_i}\right)^{-1} \tag{9}$$

an effective particle diameter $d_p = 0.228$ mm follows. In Eq. (9) w_i represents the mass fraction of particles between two sieves with diameter d_1 and d_2, and d_i the geometric mean of the two sieves, or $\sqrt{d_1 d_2}$.

After each experiment the sand was removed and the tube cleaned and dried. For each experiment, new and dried sand was used, so that an initial water saturation of zero was ensured. Both ends of the tube were sealed with removable nylon plates with inlet connections and mounted filter screens to prevent the passage of sand.

Before the steam injection experiments were run, the permeability of the dry sand bed was determined by measuring the pressure drop of air flow across the sand pack for various flow rates and pressure drops. The Reynolds number ranged from 1.2 to 2.2. The permeability was determined via

$$\kappa = \frac{4\eta_a P_{in} L \phi_{in}}{\pi D_i^2 (P_{in}^2 - P_0^2)}, \tag{10}$$

which takes into account the compressibility of the air. ϕ_{in} is the volume flow rate at the entrance of the column. The permeability of the packed beds ranged from 6.6×10^{-11} m^2 to 8.6×10^{-11} m^2 and the porosity from 43 to 45 percent; see Table 3. The porosity was determined by comparing the bulk density of the packed column and the density of the sand. In Table 4 the physical properties of the sand are tabulated. With the porosity and the effective particle diameter (see Eq. (9)), the permeability can also be computed with the Kozeny–Carman equation (Buchlin and Stubos, 1991):

$$\kappa = \frac{d_p^2 \phi^3}{181(1-\phi)^2} \tag{11}$$

In Table 3 the computed κ are also included. One can see the fair agreement between the κ values based on the air flow measurements and the κ values based on the particle size distribution and the Kozeny–Carman equation. In what follows the values obtained with the air flow measurements will be employed.

During the steam injection experiments, to prevent heat losses to the surroundings, approximately 20 mm of insulation was wrapped around the tube. A small stripe was uncovered to permit visual inspection and determination of the steam front. Immediately after the front, in the region passed by, by the front, this small stripe was closed with insulation as well. As soon as the steam front had attained the top of the tube, the steam injection was stopped.

In a low-pressure steam generator distilled water was evaporated, providing steam with a maximum absolute pressure of 4 bar. This steam was reduced in pressure, and premature condensation of the superheated steam in the supply channels (ID 0.25 in.) was prevented by electrical resistance heating.

Dry steam was injected with an absolute inlet pressure of 1.2 bar. With a thermometer the steam temperature at the entrance of the tube was measured, showing a slight and negligible superheat of the steam (of order 3°C).

The initial temperature T_0 of the sand pack was around 20°C. The ambient pressure P_0 was measured with a mercury barometer and ranged from 1.004 to 1.024 bar.

In Figs. 3 and 4 the experimentally observed position of the steam front is depicted against the elapsed time for the experiments with tube I and II, respectively. One can see that the position of the steam front by good approximation varies with the square root of time indeed for all experiments. This remark is in qualitative agreement with the theory; see Eq. (2). In the next section the measured results are compared quantitatively with theory.

The effective permeability of sand bed with condensate, $\kappa_{rv}\kappa$, was measured 24 hours after the experiment by measuring the pressure drop of air in the wet column at ambient temperature, yielding values of κ_{rv} ranging from 0.54 to 0.73 (Table 3). This procedure is acceptable as Piquemal (1994) concluded that air–water relative permeabilities at room temperature are in accordance indeed with steam–water relative permeabilities at elevated temperatures.

The amount of condensate in the tube was computed by measuring the increase in weight of the tube due to the condensation of water. From this information experimentally determined values of the water saturation were obtained, which are listed in Table 3.

The relative permeability and water saturation are generally related by:

$$\kappa_{rv} = (1 - S_l)^n \tag{12}$$

With κ_{rv} and S_l known ($S_l = S_{lc}$, since $S_{l0} = 0$), n can be computed with the help of Eq. (12), the result is included in Table 3. One can see that the magnitude of n is in the range found in the literature (Buchlin and Stubos, 1991; Falta et al., 1992). Note that $1 - S_l$ corresponds to S_v.

These measured water saturations are in fact averaged values within the tube. In order to investigate the homogeneity of the water saturation in the sand pack, and possible transport of water, a fifth experiment was executed with tube II. To create a larger amount of condensate, the sand was densely packed ($\phi = 0.41$) by intense vibrating and the tube was not insulated. During the experiment it was verified that the steam front is planar. The maximum distance between foremost and hindmost front position amounted to only a few mm.

After the experiment the average water saturation was determined in the same way as for experiments 1–4; see Table 5. In addition, after the tube cooled down, samples of the sand were taken at the bottom (where the injection takes place), the middle and the top of the tube. By drying these samples (105°C)

Table 3 Experimental data and computed κ, n, and S_{lc}

Exp	κ [m^2]	κ_{rv}	ϕ	S_{lc}	β	κ [m^2]	n	S_{lc}
	Experiments					Eq. (11)	Eq. (12)	Eq. (18)
1	7.4×10^{-11}	0.54	0.45	0.133	1.150	8.6×10^{-11}	4.24	0.126
2	6.6×10^{-11}	0.62	0.45	0.140	1.148	8.6×10^{-11}	3.12	0.128
3	8.6×10^{-11}	0.73	0.44	0.146	1.293	7.8×10^{-11}	2.04	0.149
4	6.7×10^{-11}	0.69	0.43	0.157	1.387	7.0×10^{-11}	2.17	0.156

Table 4 Properties of quartz sand, air, and glass tube

	Sand	Air	Glass
k, W/mK	8.8	0.0257	1.17
ρ, kg/m^3	2650	1180	2500
c_p, J/gK	1000	1007	840

and measuring the weight loss, the water saturation at these three locations is obtained. In Table 5 the results are summarized.

The values of Table 5 indicate that indeed the water saturation is higher than with experiments 1 and 4, due to greater heat loss. Furthermore, one can see that the water saturation is practically constant in the tube, confirming a prediction of the presented model. Table 5 also shows that, even for the large water saturation, no water has been transported as a slug ahead of the front. This contrasts with the experiments of Nilson and Montoya (1980), Tsuruta et al. (1988), and Hanamura and Kaviany (1995), who observed a liquid slug. Obviously, here the water saturation is still smaller than the irreducible saturation. This observation of S_{ir} being larger than 0.21 corresponds with values of S_{ir} found in the literature (Buchlin and Stubos, 1991). As water has not been swept for $S_l \approx 0.21$, it can be assumed that this was not the case either in experiments 1–4 where $S_l < 0.16$. This conclusion is confirmed by the observation during experiments 1 to 5 that no water was leaving the column at the exit. The immobile water phase formed a major assumption of the one-phase flow model of Brouwers and Li (1994).

In order to determine the temperature in the dry sand ahead of the front, two experiments have been performed with five equidistant thermocouples placed in the center of the sand pack. The measurements revealed that the dry sand is at ambient temperature up to the moment the steam front passes by. So, in the column a sharp temperature rise occurs at the steam front, implying negligible axial conduction ahead of the front.

Model Validation

In order to compare the theory with the experimental data, the properties appearing in a_1 and a_2 need be assessed. Both in a_1 and a_2 several physical properties appear. In a_2 also the effective permeability $\kappa_{rv}\kappa$ figures, which was obtained experimentally with the help of the air flow–pressure drop measurements 24 hours after the experiment, as explained in the previous section.

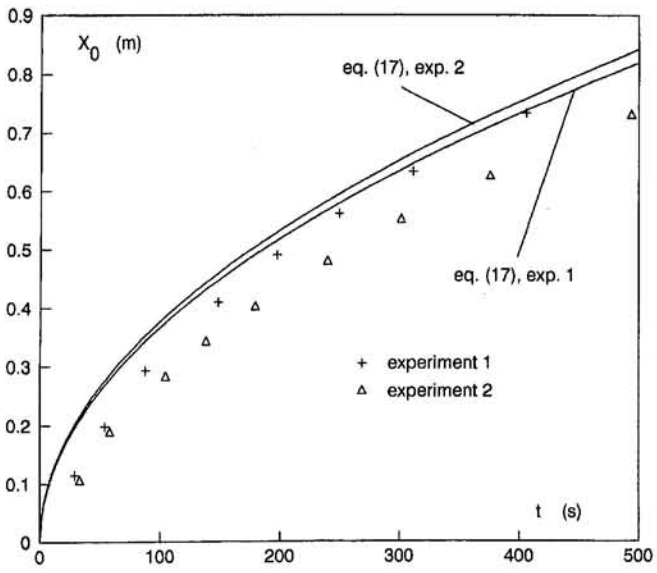

Fig. 3 The experimentally measured steam front position in tube I and the pertaining theoretical predictions

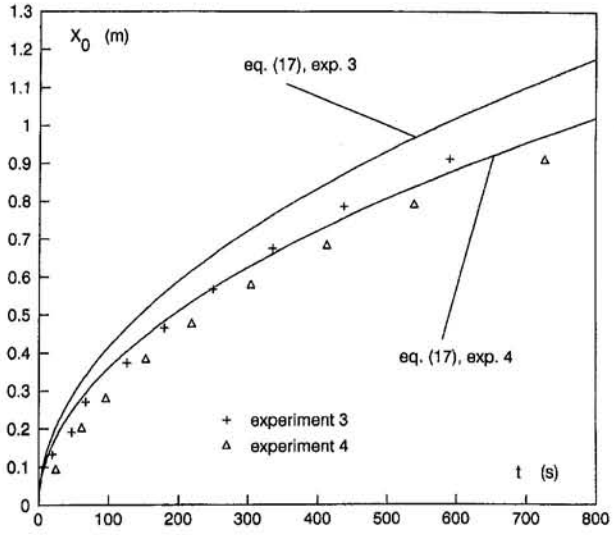

Fig. 4 The experimentally measured steam front position in tube II and the pertaining theoretical predictions

The physical properties appearing in a_1 were evaluated at P_0 and T_0 (ambient conditions), as these conditions prevail ahead of the front. The effective thermal conductivity $\overline{k}_s$ is computed with the model of Zehner and Schlünder (1970). This procedure yields values of $\overline{k}_s$ of 0.270 W/mK to 0.301 W/mK. The mean heat capacity $\overline{\rho_s c_{ps}}$ is obtained by adding the weighed contributions of sand and air. Both $\overline{k}_s$ and $\overline{\rho_s c_{ps}}$ depend on the porosity of the packed sand.

The properties appearing in a_2 were evaluated at the mean conditions between entrance and steam front, i.e., $(P_{in} + P_0)/2 (\approx 1.1$ bar) and T_{sat} (depends on P_0, $T_{sat} \approx 100°C$). The physical properties of the steam were taken from V.D.I. (1991).

With a_1 and a_2 known, y was computed to have a value ranging from 40 to 47. Subsequently, values of λ greater than 0.999 followed from Eq. (3). These values of λ, which are nearly unity, imply that all liberated latent heat at the front is available for heating up the sand pack, and that axial heat losses are negligible (Brouwers and Li, 1994). This result is in agreement with the measured temperature profile in the dry sand.

A first comparison of experimental data with theory showed that the progress of the front is slower than expected theoretically. This can be explained by the heat needed to heat up the walls of the glass tube and heat loss to the surroundings. This supposition is confirmed by the fact that the theoretical S_{lc}, following from Eq. (8), equals about 0.11. Table 3 reveals that after the experiment, depending on the used tube, $S_{lc} = 0.13$–0.16 is measured. This result implies that more steam has condensed than is needed for heating up the sand pack. One can also see that this effect is more pronounced for the thick-walled tube. Accordingly, a modification of the theory is presented to take account of the heating up of the glass tube.

Table 5 Measured average water saturation, and water saturation at three positions in the tube (experiment 5)

Tube	S_{lc}
Average	0.194
Bottom	0.219
Middle	0.189
Top	0.204

As has been said, $\lambda \approx 1$, implying that all liberated latent heat is used to heat up the sand and the glass tube at the front. An energy balance at the front yields:

$$\rho_v u_v H_{lat} = \overline{\rho_s c}_{ps} \beta (T_{sat} - T_0) \frac{dX_0}{dt} \tag{13}$$

In this equation the term β reckons with the heating up of the glass tube:

$$\beta = 1 + \frac{\rho_g c_{pg}}{\overline{\rho_s c}_{ps}} \left[\frac{D_o^2}{D_i^2} - 1 \right] \tag{14}$$

The steam flow to the front obeys Darcy's law:

$$\frac{X_0 u_v \eta_v}{\kappa_{rv} \kappa} = P_{in} - P_0 \tag{15}$$

Combining Eqs. (13) and (15), inserting Eq. (6), solving the differential equation, and applying the initial condition

$$X_0|_{t=0} = 0 \tag{16}$$

yields:

$$X_0 = \left(\frac{a_2 t}{\beta} \right)^{1/2} \tag{17}$$

The amount of condensed water in the porous medium can be obtained from an energy balance of liberated latent heat and heat required to heat up packed sand and tube wall, yielding:

$$S_{lc} = \frac{\overline{\rho_s c}_{ps} (T_{sat} - T_0) \beta}{H_{lat} \phi \rho_l} \tag{18}$$

Equations (17) and (18) are modifications of Eqs. (2) and (8), respectively, and account for the heating-up of the tube wall in case $\lambda = 1$. That is, $\lambda = 1$ when the thermal conductivity ahead of the front (or resistance to vapor flow) is negligibly small. In Table 3 β is given for both tubes, confirming that β is highest for the experiments with the thick-walled tube.

Note that axial conduction in the glass tube, as well as the sand bed, can be neglected. This can be verified by considering the poor thermal conductivity of the pyrex glass (Table 4).

Now it is possible to compare the theoretical prediction of the steam front position (Eq. (17)) with the experimental observations. In Fig. 3 the results of experiments 1 and 2 with tube I are presented with the applicable theoretical predictions. In Fig. 4 experiments 3 and 4 with tube II are summarized. The theoretical lines do not coincide as for each experiment ϕ, κ, κ_{rv}, etc. (and hence also a_2) have different values.

One can readily see that the theoretical predictions of the position of the steam front agree well, at least qualitatively, with the observed position. Particularly for the experiments with tube II, there is good agreement. The worst prediction of the steam front is found with experiment 2, and corresponds to the worst agreement between the predicted and measured amounts of condensate; see Table 3. A part of the discrepancy can be attributed to the inaccuracy of the measurements. The uncertainty analysis in the appendix reveals that the maximum relative error of the front position, dX_0/X_0, is 7.5 percent.

Conclusions

In this paper the constant-pressure steam injection into a dry and air-saturated porous medium has been investigated experimentally. To measure the vertical upward flow of the steam front, a test setup and two vertical glass tubes packed with quartz sand have been used.

A comparison of the experimental results reveal that the conduction ahead of the front can be neglected. Furthermore, the heating of the glass walls, on the other hand, has a substantial effect on the steam front position and amount of condensed water.

In order to account for this effect, a simple modification of the theory by Brouwers and Li (1994) is proposed. A comparison of the predicted steam front position and condensed water by this modified theory with the experimental result yields fairly good agreement.

Furthermore, it has been verified that the water saturation remains below the irreducible saturation and is homogeneously distributed in the sand pack. These features formed the basis of and were predicted by, respectively, the one-phase flow model of Brouwers and Li (1994).

Acknowledgments

The author is indebted to Messrs. A. F. B. Zijlstra and H. Menkehorst, who performed the experimental runs.

References

Brouwers, H. J. H., and Li, S., 1994, "An Analysis of Constant Pressure Steam Injection in an Unsaturated Porous Medium," *Proc. 10th Int. Heat Transfer Conf.*, G. F. Hewitt, ed., Brighton, Vol. 5, pp. 219–224.

Buchlin, J. M., and Stubos, A., 1991, "Phase Change Phenomena at Liquid Saturated Self Heated Particulate Beds," in: *Modelling and Applications of Transport Phenomena in Porous Media*, Chap. 3, J. Bear and J. M. Buchlin, eds., Kluwer Academic Publishers, Dordrecht.

Fair, G. M., and Hatch, L. P., 1933, "Fundamental Factors Governing Streamline Flow of Water Through Sand," *J. Am. Water Works*, Vol. 25, pp. 1551–1565.

Falta, R. W., Pruess, K., Javandel, I., and Witherspoon, P. A., 1992, "Numerical Modeling of Steam Injection for the Removal of Nonaqueous Phase Liquids From the Subsurface. 2. Code Validation and Application," *Water Resources Research*, Vol. 28, pp. 451–465.

Hanamura, K., and Kaviany, M., 1995, "Propagation of Condensation Front in Steam Injection Into Dry Porous Media," *Int. J. Heat Mass Transfer*, Vol. 38, pp. 1377–1386.

Holman, J. P., 1978, *Experimental Methods for Engineers*, 3rd ed., McGraw-Hill, New York.

Kline, S. J., and McClintock, F. A., 1953, "Describing Uncertainties in Single-Sample Experiments," *Mech. Eng.*, Vol. 75, Jan., pp. 3–8.

Mandl, G., and Volek, C. W., 1969, "Heat and Mass Transport in Steam-Drive Processes," *Soc. Pet. Eng. J.*, Mar., pp. 59–79.

Marx, J. W., and Langenheim, R. H., 1959, "Reservoir Heating by Hot Fluid Injection," *Trans. AIME*, Vol. 216, pp. 312–315.

Menegus, D. K., and Udell, K. S., 1985, "A Study of Steam Injection Into Water Saturated Capillary Porous Media," ASME HTD-Vol. 46, pp. 151–157.

Morrison, F. A., 1973, "Transient Multiphase Multicomponent Flow in Porous Media," *Int. J. Heat Mass Transfer*, Vol. 16, pp. 2331–2342.

Nilson, R. H., and Montoya, P. C., 1980, "Experiments on Transient Condensing Flow Through a Porous Medium," ASME JOURNAL OF HEAT TRANSFER, Vol. 102, pp. 489–494.

Piquemal, J., 1994, "Saturated Steam Relative Permeabilities of Unconsolidated Porous Media," *Transport in Porous Media*, Vol. 17, pp. 105–120.

Ramey, H. J., 1959, Discussion on the paper by Marx and Langenheim, *Trans. AIME*, Vol. 216, pp. 364–365.

Stewart, L. D., Basel, M. D., and Udell, K. S., 1989, "The Effect of Gravity on Steam Propagation in Porous Media," ASME HTD-Vol. 91, pp. 31–42.

Tsuruta, T., Narazaki, K., and Masuoka, T., 1988, "Transient Condensing Two-Phase Flow Through an Initially Subcooled Porous Medium," *JSME Int. J.*, Series II, Vol. 31, pp. 81–87.

V. D. I., 1991, *V. D. I. Wärmeatlas (6. Aufl.)*, V. D. I. Verlag GmbH, Düsseldorf [in German].

Zehner, P., and Schlünder, E. U., 1970, "Wärmeleitfähigkeit von Schüttungen bei mäßigen Temperaturen," *Chemie Ing. Techn.*, Vol. 42, pp. 933–941 [in German].

APPENDIX

Uncertainty Analysis

The uncertainty analysis presented here follows the procedures described by Kline and McClintock (1953) and Holman (1978). The primary experimental data, such as P_0, P_{in}, and T_0 are used to calculate the desired (dimensionless) quantities a_1, a_2, y, λ, and $X_0(t)$. The uncertainty in these calculated results is obtained by considering the uncertainties in the primary measurements and is discussed below.

The uncertainty in a calculated result I, which is a function of the independent variables $i_1, i_2, \ldots, i_n$, reads:

$$\left[\frac{dI}{I}\right]^2 = \left[\frac{\partial I}{\partial i_1}\frac{di_1}{I}\right]^2 + \left[\frac{\partial I}{\partial i_2}\frac{di_2}{I}\right]^2 + \ldots + \left[\frac{\partial I}{\partial i_n}\frac{di_n}{I}\right]^2 \tag{A.1}$$

where $di_1, di_2, \ldots, di_n$ represent the uncertainties in the quantities $i_1, i_2, \ldots, i_n$.

The uncertainty in a_2, denoted by da_2, depends on $d\kappa_{rv}\kappa$, $d\rho_s c_{ps}$, dP_0, dP_{in}, dT_{sat}, dT_0, dH_{lat}, and $d\nu_v$; see Eq. (6). The effective permeability of the wet sand $\kappa_{rv}\kappa$ is measured separately via flow and pressure drop measurements; see Eq. (10). Uncertainties in the physical properties, geometric properties, ambient pressure, and temperatures are much smaller than the uncertainty of the inlet pressure and gas flow, and are therefore neglected. Application of Eq. (A.1) to a_2 and $\kappa_{rv}\kappa$ produces:

$$\left[\frac{da_2}{a_2}\right]^2 = \left[\frac{dP_{in}}{P_{in} - P_0}\right]^2 + \left[\frac{d\kappa_{rv}\kappa}{\kappa_{rv}\kappa}\right]^2 \tag{A.2}$$

$$\left[\frac{d\kappa_{rv}\kappa}{\kappa_{rv}\kappa}\right]^2 = \left[\frac{P_{in}^2 + P_0^2}{P_{in}^2 - P_0^2}\right]^2 \left[\frac{dP_{in}}{P_{in}}\right]^2 + \left[\frac{d\phi_{in}}{\phi_{in}}\right]^2 \tag{A.3}$$

P_{in} and P_0 in Eq. (A.2) reflect the pressures during the steam front measurements (pressure drop amounts to 0.2 bar). P_{in} and P_0, appearing in Eq. (A.3), are the pressures during the air flow measurements, which took place 24 hours after the steam front measurement ($P_{in} - P_0$ is about 1.4 bar).

The inaccuracy in front position is mainly caused by the inaccuracy in a_2. Applying Eq. (A.1) to Eq. (2) yields:

$$\frac{dX_0}{X_0} = \frac{da_2}{2a_2} \tag{A.4}$$

With the help of Eqs. (A.2)-(A.4) the relative inaccuracy of the lines drawn in Figs. 3 and 4 can now be assessed. This uncertainty is much larger than the uncertainty in measured front position and time, which are depicted in both figures as discrete symbols.

The gas flow is measured with the aid of a rotameter with an inaccuracy $d\phi_{in}$ of 100 l/h, and the inlet pressure with a bourdon pressure gage with an inaccuracy dP_{in} of 0.02 bar. Hence, for the experimental data of Figs. 3 and 4 the maximum dX_0/X_0 amounts to 0.075.